Journal of Nuclear Medicine, published on September 25, 2020 as doi:10.2967/jnumed.120.249367

Repurposing [^{11}C]PS13 for PET imaging of cyclooxygenase-1 (COX-1) in ovarian cancer xenograft mouse models

Amanda J. Boyle[1, †], Junchao Tong[1], Sami S. Zoghbi[2], Victor W. Pike[2], Robert B. Innis[2], and Neil Vasdev[1,3,*]

[1]*Azrieli Centre for Neuro-Radiochemistry, Brain Health Imaging Centre, Centre for Addiction and Mental Health, Toronto, Ontario, M5T-1R8, Canada*

[2]*National Institute of Mental Health, Bethesda, Maryland, USA*

[3]*Department of Psychiatry, University of Toronto, Toronto, Ontario, M5T-1R8, Canada*

* Corresponding author:

Email address: neil.vasdev@utoronto.ca (N. Vasdev)

Tel.: +1 416 535 8501 extension 30988

[†]First author:

Email address: amy.boyle@camh.ca (A.J. Boyle)

Tel.: +1 416 535 8501 extension 30884

ABSTRACT

Cyclooxygenase-1 (COX-1), a biomarker for neuroinflammation, is implicated in ovarian cancer (OvCa) progression and prognosis. This study considered the repurposing of [^{11}C]PS13, a COX-1 PET neuroimaging radiopharmaceutical, in OvCa xenograft mouse models. **Methods:** [^{11}C]PS13 was evaluated in ICRscid mice with s.c. or i.p. human OVCAR-3 OvCa xenografts by dynamic PET/MR imaging, *ex vivo* biodistribution and radiometabolite analysis of plasma and tumor. **Results:** OVCAR-3 xenografts were well visualized with [^{11}C]PS13 in xenograft mouse models. Time-activity curves revealed steady tumor radioactivity accumulation that plateaued from 40-60 min, and was significantly reduced by pre-treatment with ketoprofen (3.56 ± 0.81 and 1.30 ± 0.18 %ID/g, respectively, p=0.01). Radiometabolite analysis showed that intact [^{11}C]PS13 accounted for >80% of radioactivity in the tumor, with <20% in plasma, at 40 min post-injection. **Conclusions:** [^{11}C]PS13 shows promise for PET imaging COX-1 in OvCa and rapid translation for clinical cancer research should be considered.

Key words: cyclooxygenase-1, ovarian cancer, repurposing, PET, carbon-11, COX-1.

INTRODUCTION

Ovarian cancer (OvCa) is the most lethal gynecological cancer, accounting for 5% of all cancer-related deaths, due to 80% of patients being diagnosed with advanced disease (*1*). Early detection of OvCa is desperately needed to improve outcomes for patients as those diagnosed at early stage have a 5-year survival rate of 93%, compared with the dire 17% for those diagnosed with metastatic disease (*1*). There are few positron emission tomography (PET) radiopharmaceuticals for OvCa in a clinical setting. The most common PET radiopharmaceutical for OvCa, 2-[^{18}F]fluoro-2-deoxy-D-glucose ([^{18}F]FDG), has downfalls including false-negative results in early stage OvCa, and false-positives when inflammatory co-morbidities are present (*2,3*). Novel biomarkers for PET imaging of OvCa are avidly pursued in preclinical research including receptor overexpression, cell proliferation, vasculature, and hypoxia (*3-10*).

In OvCa, cyclooxygenase-1 (COX-1) overexpression is associated with poor prognosis, tumorigenesis, and tumor invasion (*11-13*). To our knowledge, the only COX-1-targeted PET imaging agent explored in preclinical oncology research is ^{18}F-labeled 3-(4-fluorophenyl)-5,5-dimethyl-4-(*p*-tolyl)furan-2(5*H*)-one ([^{18}F]FDF; IC_{50}=220 nM) (*14*). Carbon-11-labeled 1,5-bis(4-methoxyphenyl)-3-(2,2,2-trifluoroethoxy)-1*H*-1,2,4-triazole ([^{11}C]PS13) is a COX-1-targeted PET radiopharmaceutical that is >200-fold more potent than [^{18}F]FDF, and has recently been translated for clinical neuroimaging research (*15-18*). This study explores the potential of repurposing [^{11}C]PS13 in rodent models of OvCa via dynamic PET imaging, *ex vivo* biodistribution studies, and radiometabolite analysis.

METHODS AND MATERIALS

Description of the radiochemical synthesis of [^{11}C]PS13 is available in supplemental materials at http://jnm.snmjournals.org (*17,19*).

Tumor Xenograft Mouse Models

OVCAR-3 human OvCa cells (American Type Culture Collection) with high COX-1 expression (*14*) were cultured in RPMI 1640 medium supplemented with 20% fetal bovine serum (Gibco, Life Technologies), 1% penicillin/streptomycin (Sigma-Aldrich), and 0.01 mg/mL bovine insulin (Sigma-Aldrich). Cells were cultured in an atmosphere of 5% CO_2 at 37°C. ICRscid mice (Taconic Biosciences), were inoculated subcutaneously (s.c.) on the right flank and imaged when

tumors reached 0.75-1.0 cm diameter, or intraperitoneally (i.p.) with 1×10^7 OVCAR-3 cells in 100 µL PBS combined with 100 µL Matrigel (Corning). Mice bearing i.p. xenografts, which are more physiologically relevant than s.c. xenografts, were imaged sporadically from Week 2 to Week 6 post-inoculation to examine the potential of [^{11}C]PS13 to detect early stage OvCa. Animal studies were conducted under a protocol (#817) approved by the Animal Care Committee at the Centre for Addition and Mental Health, following Canadian Council on Animal Care guidelines. Male mice were used to generate s.c. models for preliminary PET imaging, while female mice were used to generate i.p. and s.c. cancer models for PET imaging and radiometabolite analysis, respectively.

PET/MR Imaging and Biodistribution Studies

PET Acquisition Method. For small animal PET combined with magnetic resonance (MR) imaging studies, mice were anesthetized by isoflurane in O_2 (4%, 2 L/min induction; 1-2%, 1 L/min maintenance) for lateral tail-vein catheterization then transferred to a nanoScan™ PET/MRI 3T scanner (Mediso). Mice (n=6) were injected through the tail-vein catheter with [^{11}C]PS13 (2.00-9.93 MBq, 1.53-9.02 nmol/kg, 11-101 GBq/µmol). A group of mice (n=2) were pre-treated with an i.p. injection of 2 mg in 20 µL dimethylsulfoxide of the COX-1 inhibitor, ketoprofen (Selleck Chemicals), 60 min prior to bolus injection of [^{11}C]PS13. Biodistribution was performed on mice bearing s.c. xenografts which were sacrificed by cervical dislocation and selected tissue samples were collected, weighed, and transferred to γ-counting tubes. Tissue radioactivity was measured with a γ-counter and expressed as %ID/g.

PET Data Analyses. Image analyses and extraction of time activity curves (TACs) in regions of interest (ROIs) were performed in Amide v1.0.4. Further details are available in the supplemental materials (*20*).

Radiometabolite Analysis

Tumor-bearing mice were sacrificed by cervical dislocation 40 min following injection with [^{11}C]PS13 (16.84-22.54 MBq, 1.72-5.84 nmol/kg, 99.5-434 GBq/µmol). Blood was collected by cardiac heart puncture then centrifuged for 5 min at 1500 × rcf. Tumors were excised and homogenized with a Polytron homogenizer (Kinematica) in 2 mL acetonitrile with 50 ng of PS13 to improve the extraction of [^{11}C]PS13 from tissue, then 1 mL H_2O was added. The homogenate

was centrifuged at 13500 × rcf for 5 min. [^{11}C]PS13 product, plasma, and tumor homogenates were separated by column-switching HPLC, as previously described, with a mobile phase of acetonitrile in 0.1 N (aq)_ammonium formate (65:35 v/v) and analyzed with PowerChrom 2.6.15 (eDAQ) (*21*).

Statistical Analysis

Data are represented as the mean ± SD. Statistical comparisons were performed by an unpaired t-test, corrected for multiple comparisons using the Bonferroni-Dunn method ($p < 0.05$) with GraphPad Prism Version 8.3.1.

RESULTS

PET/MR Imaging of OVCAR-3 Tumor-Bearing Mice

We evaluated [^{11}C]PS13 in ICRscid mice bearing s.c. or i.p. OVCAR-3 xenografts. Fig. 1A shows representative static PET images in which tumors were visualized with [^{11}C]PS13 (0-60 min average image). Fig. 1B depicts representative PET images of tumor-bearing mice pre-treated with ketoprofen, showing reduced tumor radioactivity accumulation which demonstrates COX-1 specificity of [^{11}C]PS13. Fig. 2 shows representative static PET images in which i.p. xenografts were visualized as early as 2 weeks post-inoculation with OVCAR-3 cells. Supplemental Fig. 1 and 2 show PET imaging data in of other i.p. xenograft mice (n=3).

TACs revealed steady tumor radioactivity accumulation that plateaued from 40-60 min with an average uptake of 3.56 ± 0.81 %ID/g (n=6), (Fig. 3A and 3B). Muscle tissue exhibited washout of radioactivity over time and the average uptake between 40 and 60 min was significantly lower than for tumor tissue (0.99 ± 0.21 %ID/g; p=0.00002), leading to a tumor-to-muscle ratio of 3.60 (Fig. 3A, B). TACs in Fig. 3C show that tumor radioactivity accumulation was significantly reduced, 63.5%, by pre-treatment with ketoprofen to 1.30 ± 0.18 %ID/g (p=0.0096). Pre-treatment with ketoprofen did not affect muscle accumulation, therefore off-target binding of [^{11}C]PS13 was not apparent (Fig. 3E and 3F). PET imaging analyses were substantiated by *ex vivo* biodistribution studies (Supplemental Fig. 3 and Supplemental Table 1). The average uptake from 40-60 min for i.p. xenograft mice was 4.78 ± 0.88 %ID/g.

Radiometabolite Analysis

Ex vivo composition of [^{11}C]PS13 in plasma and tumor tissue was determined at 40 min p.i. (based on plateau in TACs) in s.c. tumor-bearing mice by HPLC analysis of relative amounts of parent radioligand and radiometabolites. At 40 min p.i. intact [^{11}C]PS13 represented 17.5 ± 1.6% of total radioactivity in the plasma and 80.6 ± 0.7% in tumor tissue (Supplemental Fig. 4 and 5). This analysis represents one time-point in compartmental modeling of the tumor; future studies will examine complete compartmental modeling with various time-points.

DISCUSSION

[^{11}C]PS13 is the most potent and selective COX-1 inhibitor reported to date and has recently been translated for human PET studies of neuroinflammation (*16*). Repurposing this PET radiopharmaceutical to OvCa imaging can greatly accelerate the timeline for translation of a COX-1 radiopharmaceutical for oncology (*22*). Herein, we report the successful PET/MR imaging of human OvCa xenografts with COX-1-targeted [^{11}C]PS13 with high accumulation of radioactivity in the tumor. TACs showed a desirable pharmacological profile of [^{11}C]PS13: radioactivity accumulated in the tumor, while remaining low in muscle tissue and washed out over time (Fig. 3A).

Target-engagement experiments showed that COX-1 mediates [^{11}C]PS13 accumulation in the tumor with a 2.7-fold decrease observed in mice pre-treated with ketoprofen (Fig. 3C). Our study demonstrated a 3-fold greater tumor accumulation with [^{11}C]PS13 than that reported for [^{18}F]FDF in a s.c. OvCa xenograft mouse model (*14*). We also demonstrated the potential of [^{11}C]PS13 to detect early stage OvCa in clinically relevant i.p. xenograft mouse models in which tumors were successfully visualized at 2 weeks post-inoculation (Fig. 2). As tumor growth inhibition has been demonstrated by COX-1 inhibitors in preclinical studies (*23*), the radiometabolite analysis showing sequestering of intact [^{11}C]PS13 in tumor tissue suggests that this radiotracer could be potentially useful for confirming target engagement and dosing regimens for non-radioactive COX-1 therapeutics in oncology. Notably, there is a lower affinity of [^{11}C]PS13 for rodent compared to human COX-1, IC_{50}=15 nM and 1 nM, respectively. Despite a lower affinity of [^{11}C]PS13 for rodent compared to human COX-1, IC_{50}=15 nM and 1 nM, respectively, a difference in [^{11}C]PS13 background between rodent and higher species is not expected because no specific

binding of [^{11}C]PS13 was observed in healthy ovarian tissue of rhesus monkeys (*15*) which is consistent with our preliminary human data (unpublished).

CONCLUSIONS

We report the successful repurposing of a COX-1 human neuroimaging agent, [^{11}C]PS13, for visualizing human OvCa tumors in s.c. and i.p. xenograft mouse models. Clinical translation of this radiopharmaceutical for early detection of OvCa is warranted.

ACKNOWLEDGEMENTS

AJB acknowledges support from the CAMH Discovery Fund. NV thanks the Azrieli Foundation, the Canada Research Chairs Program, Canada Foundation for Innovation and the Ontario Research Fund for support. SSZ, VWP, and RBI were supported by the Intramural Research Program of the National Institutes of Health (NIMH; project numbers ZIA-MH002793, ZIA-MH002795, and ZIAMH002852).

DISCLOSURE

No potential conflicts of interest relevant to this article exist.

KEY POINTS

QUESTION: Can a COX-1 targeted neuro-PET imaging radiopharmaceutical be repurposed for the detection of OvCa?

PERTINENT FINDINGS: This study showed that [^{11}C]PS13 could visualize OVCAR-3 OvCa tumors in s.c. and physiologically relevant i.p. xenograft mouse models with excellent target specificity.

IMPLICATIONS FOR PATIENT CARE: The radiopharmaceutical [^{11}C]PS13 may be rapidly translated for human PET imaging of OvCa.

REFERENCES

1. Torre LA, Trabert B, DeSantis CE, et al. Ovarian cancer statistics, 2018. *CA Cancer J Clin.* 2018;68:284-296.

2. Park T, Lee S, Park S, et al. Value of [^{18}F]FDG PET/CT in the detection of ovarian malignancy. *Nucl Med Mol Imaging.* 2015;49:42-51.

3. Khiewvan B, Torigian DA, Emamzadehfard S, et al. An update on the role of PET/CT and PET/MRI in ovarian cancer. *Eur J Nucl Med Mol Imaging.* 2017;44:1079-1091.

4. Antunes IF, van Waarde A, Dierckx RA, de Vries EG, Hospers GA, de Vries EF. Synthesis and evaluation of the estrogen receptor beta-selective radioligand 2-[^{18}F]fluoro-6-(6-hydroxynaphthalen-2-yl)pyridin-3-ol: Comparison with 16alpha-[^{18}F]F-fluoro-17beta-estradiol. *J Nucl Med.* 2017;58:554-559.

5. Makvandi M, Pantel A, Schwartz L, et al. A PET imaging agent for evaluating PARP-1 expression in ovarian cancer. *J Clin Invest.* 2018;128:2116-2126.

6. Ocak M, Gillman AG, Bresee J, et al. Folate receptor-targeted multimodality imaging of ovarian cancer in a novel syngeneic mouse model. *Mol Pharm.* 2015;12:542-553.

7. Tsuyoshi H, Morishita F, Orisaka M, Okazawa H, Yoshida Y. 18F-fluorothymidine PET is a potential predictive imaging biomarker of the response to gemcitabine-based chemotherapeutic treatment for recurrent ovarian cancer: preliminary results in three patients. *Clin Nucl Med.* 2013;38:560-563.

8. Trencsényi G, Márián T, Lajtos I, et al. [^{18}F]FDG, [^{18}F]FLT, [^{18}F]FAZA, and ^{11}C-methionine are suitable tracers for the diagnosis and in vivo follow-up of the efficacy of chemotherapy by miniPET in both multidrug resistant and sensitive human gynecologic tumor xenografts. *Biomed Res Int.* 2014;2014:787365.

9. Li F, Zhang Z, Cai J, et al. Primary preclinical and clinical evaluation of ^{68}Ga-DOTA-TMVP1 as a novel VEGFR-3 PET imaging radiotracer in gynecological cancer. *Clin Cancer Res.* 2020;26:1318-1326.

10. Sharma R, Valls PO, Inglese M, et al. [^{18}F]Fluciclatide PET as a biomarker of response to combination therapy of pazopanib and paclitaxel in platinum-resistant/refractory ovarian cancer. *Eur J Nucl Med Mol Imaging.* 2020;47:1239-1251.

11. Beeghly-Fadiel A, Wilson AJ, Keene S, et al. Differential cyclooxygenase expression levels and survival associations in type I and type II ovarian tumors. *J Ovarian Res.* 2018;11:17.

12. Wilson AJ, Fadare O, Beeghly-Fadiel A, et al. Aberrant over-expression of COX-1 intersects multiple pro-tumorigenic pathways in high-grade serous ovarian cancer. *Oncotarget.* 2015;6:21353-21368.

13. Lau MT, Wong AS, Leung PC. Gonadotropins induce tumor cell migration and invasion by increasing cyclooxygenases expression and prostaglandin E(2) production in human ovarian cancer cells. *Endocrinology.* 2010;151:2985-2993.

14. Uddin MJ, Wilson AJ, Crews BC, et al. Discovery of furanone-based radiopharmaceuticals for diagnostic targeting of COX-1 in ovarian cancer. *ACS Omega.* 2019;4:9251-9261.

15. Kim MJ, Shrestha SS, Cortes M, et al. Evaluation of two potent and selective PET radioligands to image COX-1 and COX-2 in rhesus monkeys. *J Nucl Med.* 2018;59:1907-1912.

16. Kim M-J, Lee J-H, Juarez Anaya F, et al. First-in-human evaluation of [^{11}C]PS13, a novel PET radioligand, to quantify cyclooxygenase-1 in brain. *Eur J Nucl Med Mol Imaging.* 2020. In press.

17. Singh P, Shrestha S, Cortes-Salva MY, et al. 3-Substituted 1,5-diaryl-1 H-1,2,4-triazoles as prospective PET radioligands for imaging brain COX-1 in monkey. Part 1: Synthesis and pharmacology. *ACS Chem Neurosci.* 2018;9:2610-2619.

18. Shrestha S, Singh P, Cortes-Salva MY, et al. 3-Substituted 1,5-diaryl-1 H-1,2,4-triazoles as prospective PET radioligands for imaging brain COX-1 in monkey. Part 2: Selection and evaluation of [^{11}C]PS13 for quantitative imaging. *ACS Chem Neurosci.* 2018;9:2620-2627.

19. Wilson AA, Garcia A, Houle S, Vasdev N. Utility of commercial radiosynthetic modules in captive solvent [^{11}C]-methylation reactions. *J Labelled Compd Radiopharm.* 2009;52:490-492.

20. Defrise M, Kinahan PE, Townsend DW, Michel C, Sibomana M, Newport DF. Exact and approximate rebinning algorithms for 3-D PET data. *IEEE Trans Med Imaging.* 1997;16:145-158.

21. Moran MD, Wilson AA, Elmore CS, et al. Development of new carbon-11 labelled radiotracers for imaging $GABA_A$- and $GABA_B$-benzodiazepine receptors. *Bioorg Med Chem*. 2012;20:4482-4488.

22. Pushpakom S, Iorio F, Eyers PA, et al. Drug repurposing: progress, challenges and recommendations. *Nat Rev Drug Discov.* 2019;18:41-58.

23. Pannunzio A, Coluccia M. Cyclooxygenase-1 (COX-1) and COX-1 Inhibitors in Cancer: A review of oncology and medicinal chemistry literature. *Pharmaceuticals (Basel)*. 2018;11:101.

FIGURES AND TABLES

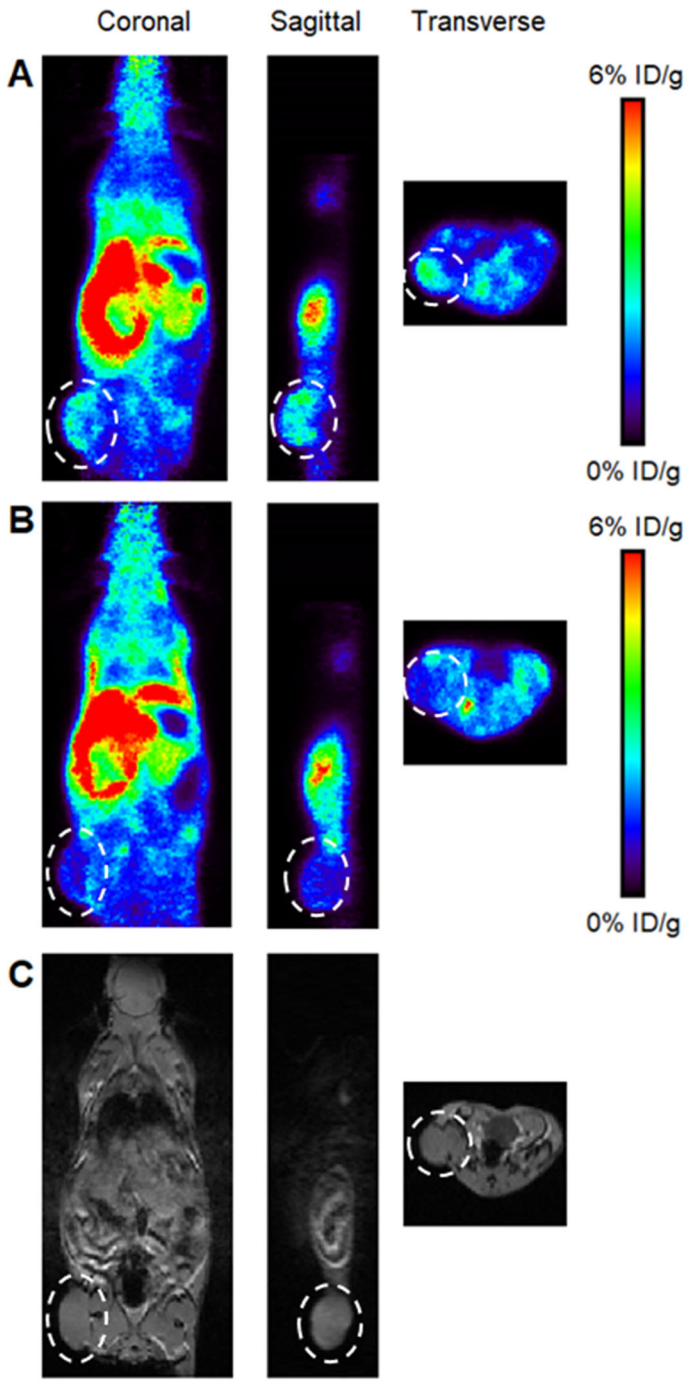

FIGURE 1. PET imaging of [^{11}C]PS13 in OVCAR-3 s.c. xenograft mice. Representative PET images of [^{11}C]PS13 under (A) baseline and (B) blocked conditions. (C) Associated MR image for (A) and (B). The tumor is indicated by white dashed circles.

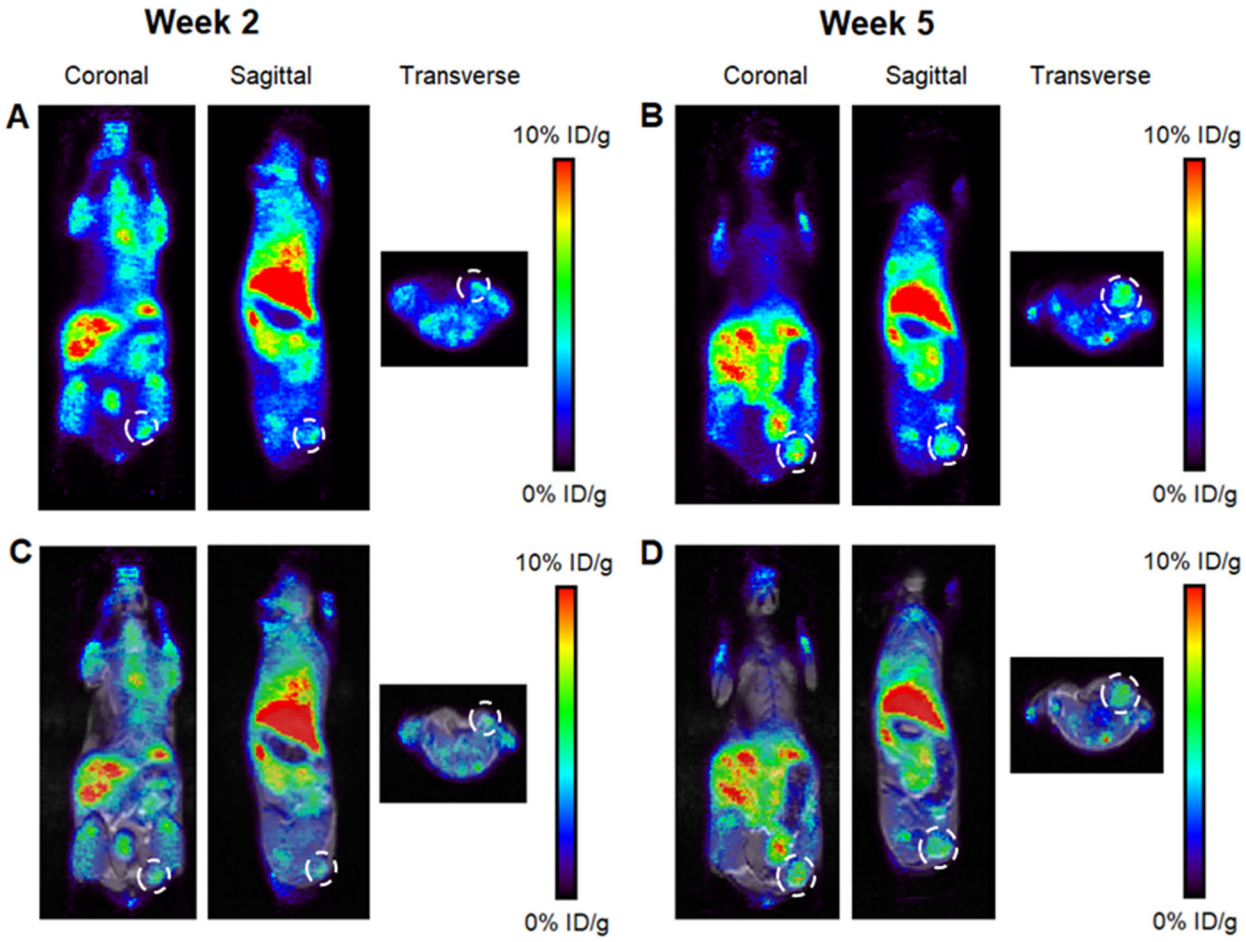

FIGURE 2. PET imaging of [^{11}C]PS13 in OVCAR-3 i.p. xenograft mouse model. PET images (A and B) and PET/MR fusion images (C and D) at week 2 and week 5 post-inoculation with cancer cells. The tumor is indicated by white dashed circles.

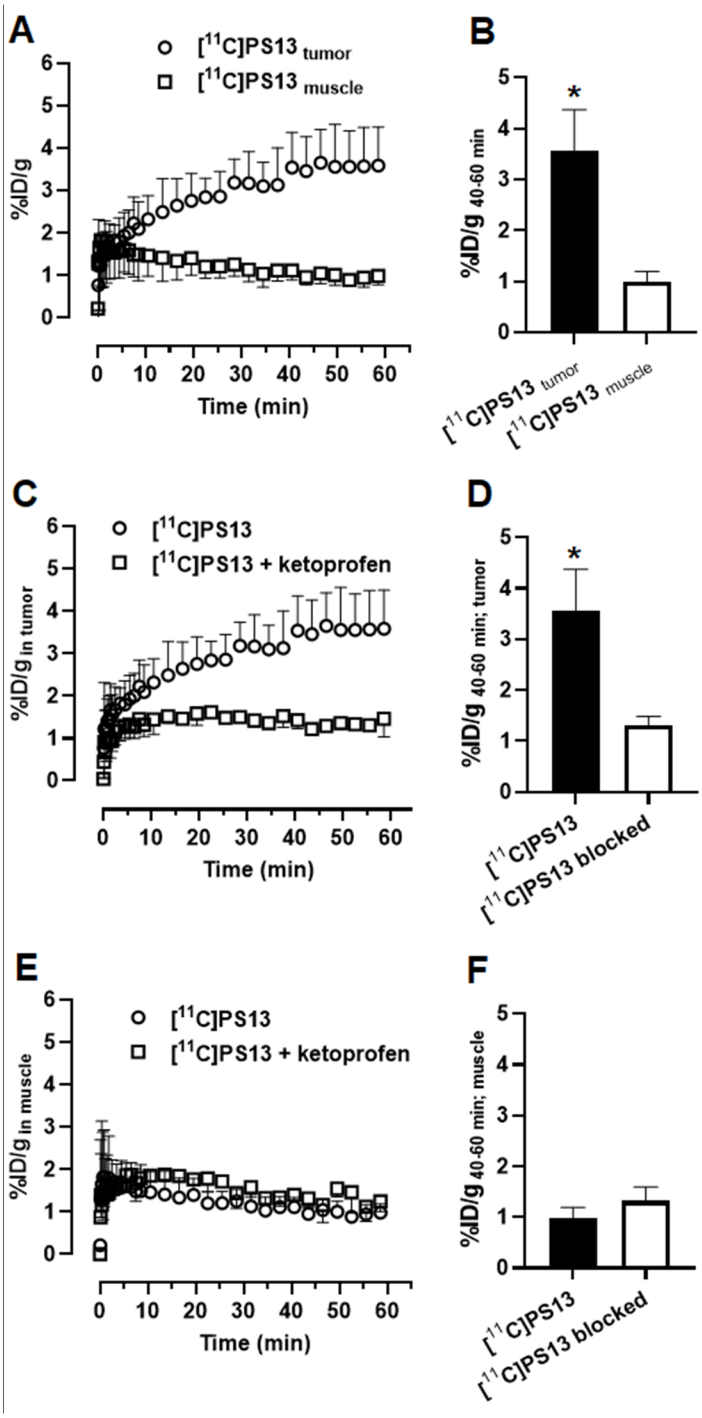

FIGURE 3. TACs of [^{11}C]PS13 in tissues of OVCAR-3 s.c. xenograft mice over 60 min. TACs of radioactivity in (A) tumor tissue and muscle tissue, (C) tumor under baseline and blocked conditions, and (E) muscle tissue under baseline and blocked conditions. (B) Average uptake 40-60 min in tumor and muscle tissue, (D) tumor under baseline and blocked conditions, and (F) muscle tissue under blocked and unblocked conditions. Asterisk (*) indicates significant differences.

Radiochemical synthesis

Desmethyl-PS13 and authentic PS13 were synthesized as previously described (*17*) and all other compounds were obtained from commercial sources. [^{11}C]PS13 was prepared using a GE Tracerlab FX2 C-Pro™ synthesis module, as previously described (*17*), with minor modifications to adapt a "loop method" (*19*). Briefly, desmethyl-PS13 (1.0 ± 0.1 mg) was dissolved in dimethylformamide (80 µL) then 1.5 µL of potassium *tert*-butoxide solution (1.0 M in tetrahydrofuran) was added. The resulting solution was injected onto a 5 mL stainless steel loop approximately 5 minutes prior to radiosynthesis. [^{11}C]iodomethane transferred to the loop and held at room temperature for 5 min prior to high pressure liquid chromatography (HPLC) purification and formulation. [^{11}C]PS13 was prepared to a molar activity of 11-101 GBq/µmol with >99% radiochemical purity.

PET/MR acquisition and analysis

PET acquisition method: With mice anesthetized and stable in the PET/MR scanner, a short gradient echo (GRE) scout MR was acquired for positioning the mouse in the PET field of view followed by a T1-weighted material map MR acquisition (GRE 3D, TR 25 ms, TE 4.76 ms) for PET and MR co-registration and PET scatter and attenuation corrections. PET scans were initiated at the time of radioligand injection and the list mode data were acquired for 60 min with an energy window of 400-600 keV.

PET data analyses: Acquired data were sorted into 33, 3D (3×5s, 3×15s, 3×20s, 7×60s, 17×180s) true sinograms (ring difference 84). 3D sinograms were converted in 2D sinograms using Fourier rebinning (*20*) with corrections for detector geometry, efficiencies, attenuation and scatter, prior to image reconstruction using a 2D-filtered back projection (FBKP) with a Hann filter at a cut-off of 0.50 cm^{-1}. A static image of the complete emission acquisition was reconstructed with the manufacturer's iterative 3D algorithm (6 subsets, 4 iterations). The static iterative image was used for PET and MR co-registration and for presentation in figures. All data were corrected for dead-time and decay corrected to the start of acquisition. Dynamic FBKP images were used to extract time-activity curves (TACs). Regions of interest (ROIs) were placed in the tumor or contralateral muscle tissue. TACs were extracted from ROIs and expressed as %ID/g, assuming tissue density of 1 g/mL.

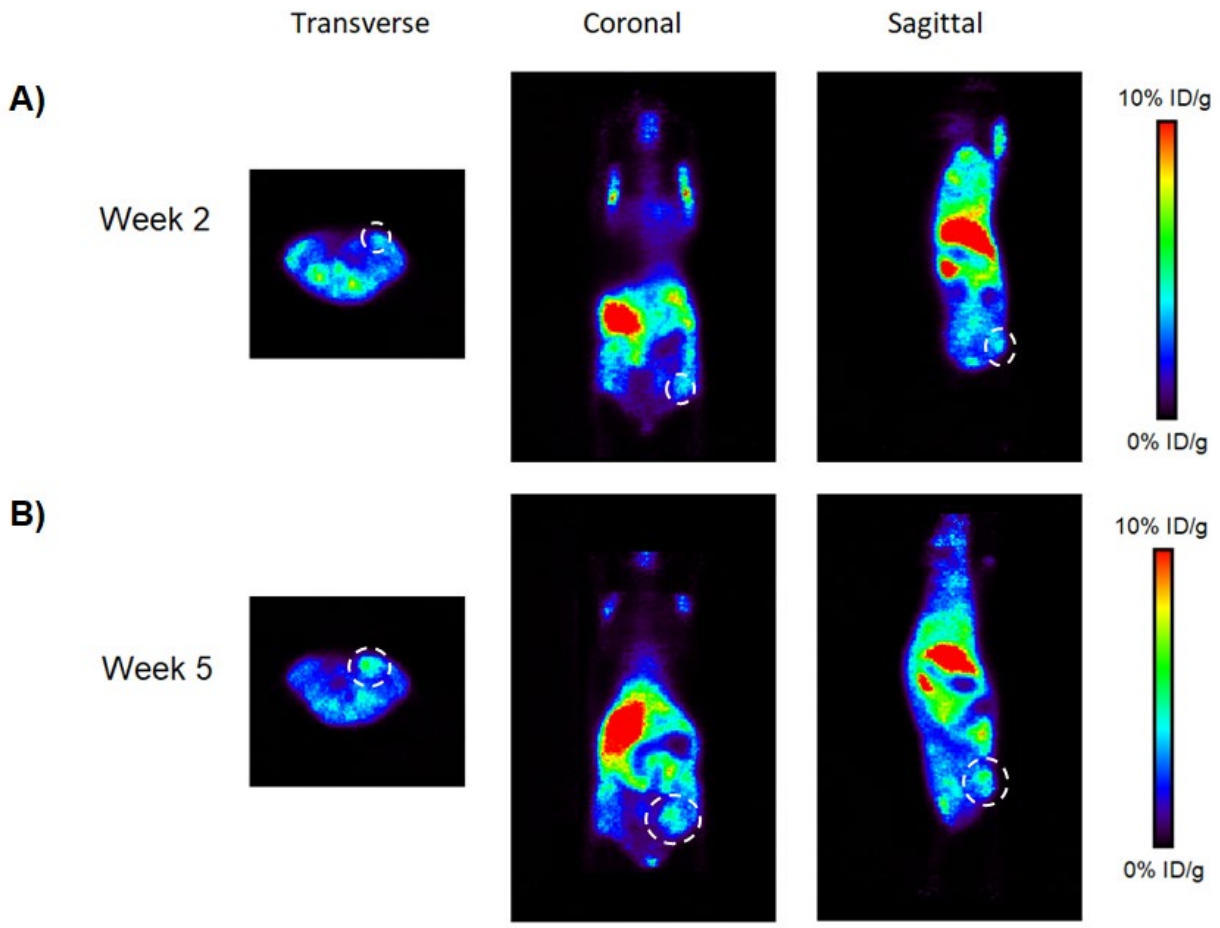

SUPPLEMENTAL FIGURE 1. PET imaging of [^{11}C]PS13 in an individual OVCAR-3 i.p. xenograft mouse (n=3). Transverse, coronal, and sagittal views of representative PET images, 0-60 min, at (A) week 2, and (B) week 5 post-inoculation.

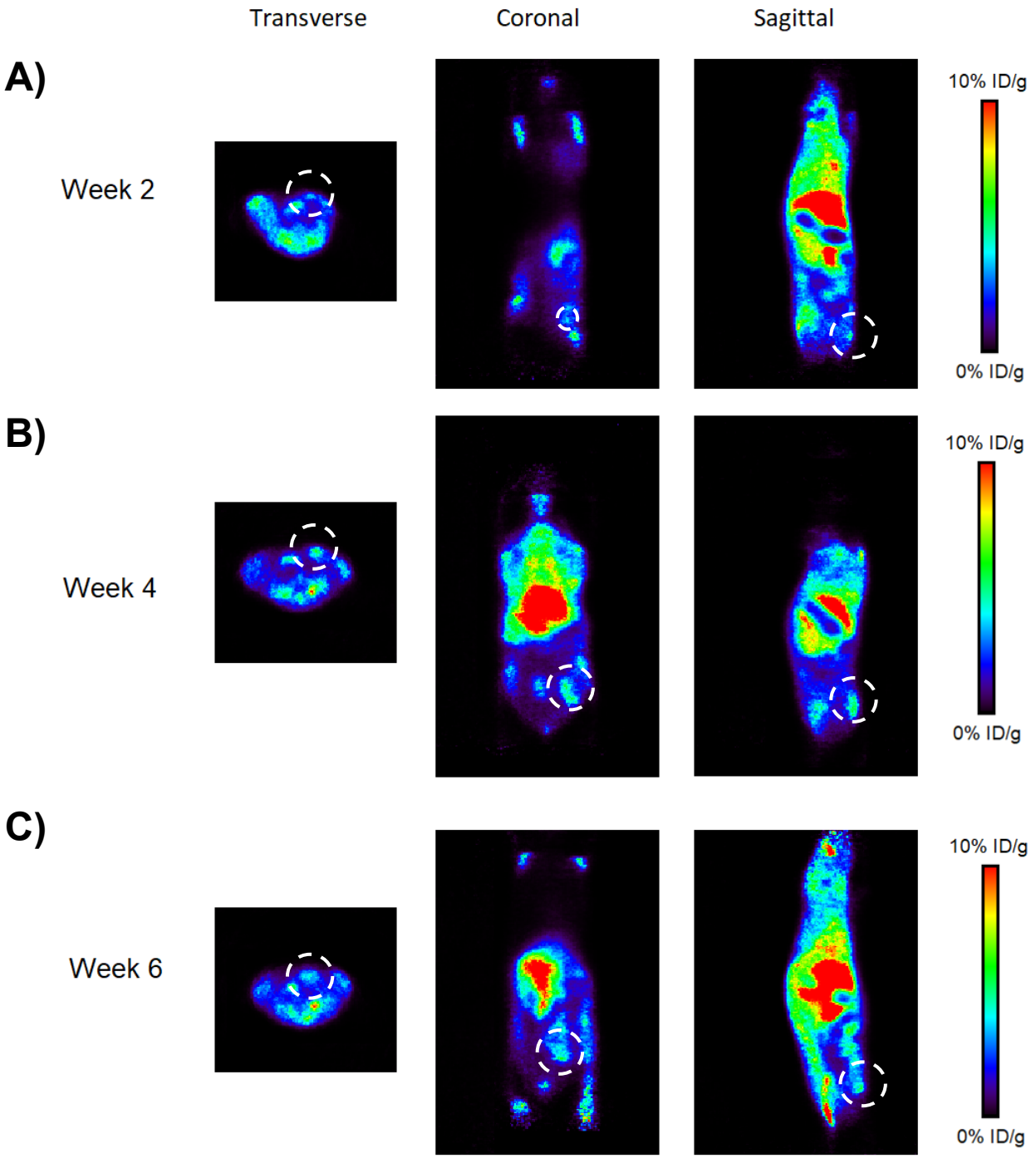

SUPPLEMENTAL FIGURE 2. PET imaging of [^{11}C]PS13 in an individual OVCAR-3 i.p. xenograft mouse (n=3). Transverse, coronal, and sagittal views of representative PET images, 0-60 min, at (A) week 2, (B) week 4, and (C) week 6 post-inoculation.

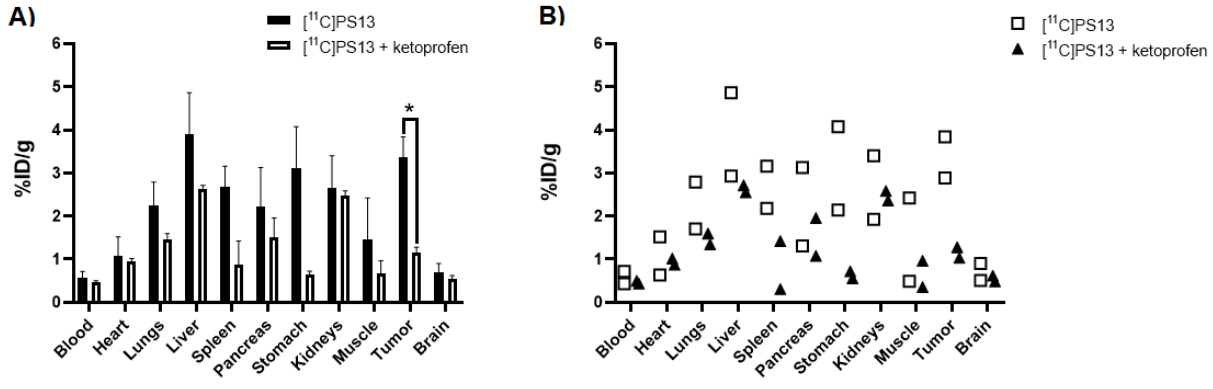

SUPPLEMENTAL FIGURE 3. *Ex vivo* biodistribution profile of [^{11}C]PS13 in OVCAR-3 tumor-bearing mice (n=2, s.c. xenograft) with and without pre-treatment with ketoprofen. (A) shows the mean ± SD; (B) shows individual mouse data. Asterisks indicate significant differences (p<0.05).

SUPPLEMENTAL TABLE 1. Validation of PET data analyses of tumor (s.c. xenograft) radioactivity accumulation by *ex vivo* biodistribution studies. No significant differences were observed for tumor radioactivity accumulation results obtained from PET image analyses compared to biodistribution studies, and significant differences were observed between baseline and blocked tumor radioactivity accumulation results for both PET image analysis and biodistribution studies.

TUMOR ACCUMULATION (%ID/G)

	PET Analysis	**Biodistribution**	***p***
[^{11}C]PS13$_{40\text{-}60\ MIN}$	3.56 ± 0.81 (n=6)	3.36 ± 0.48 (n=2)	0.76
[^{11}C]PS13 + KETOPROFEN$_{40\text{-}60\ MIN}$	1.30 ± 0.18 (n=2)	1.16 ± 0.12 (n=2)	0.46
P	0.00096	0.046	

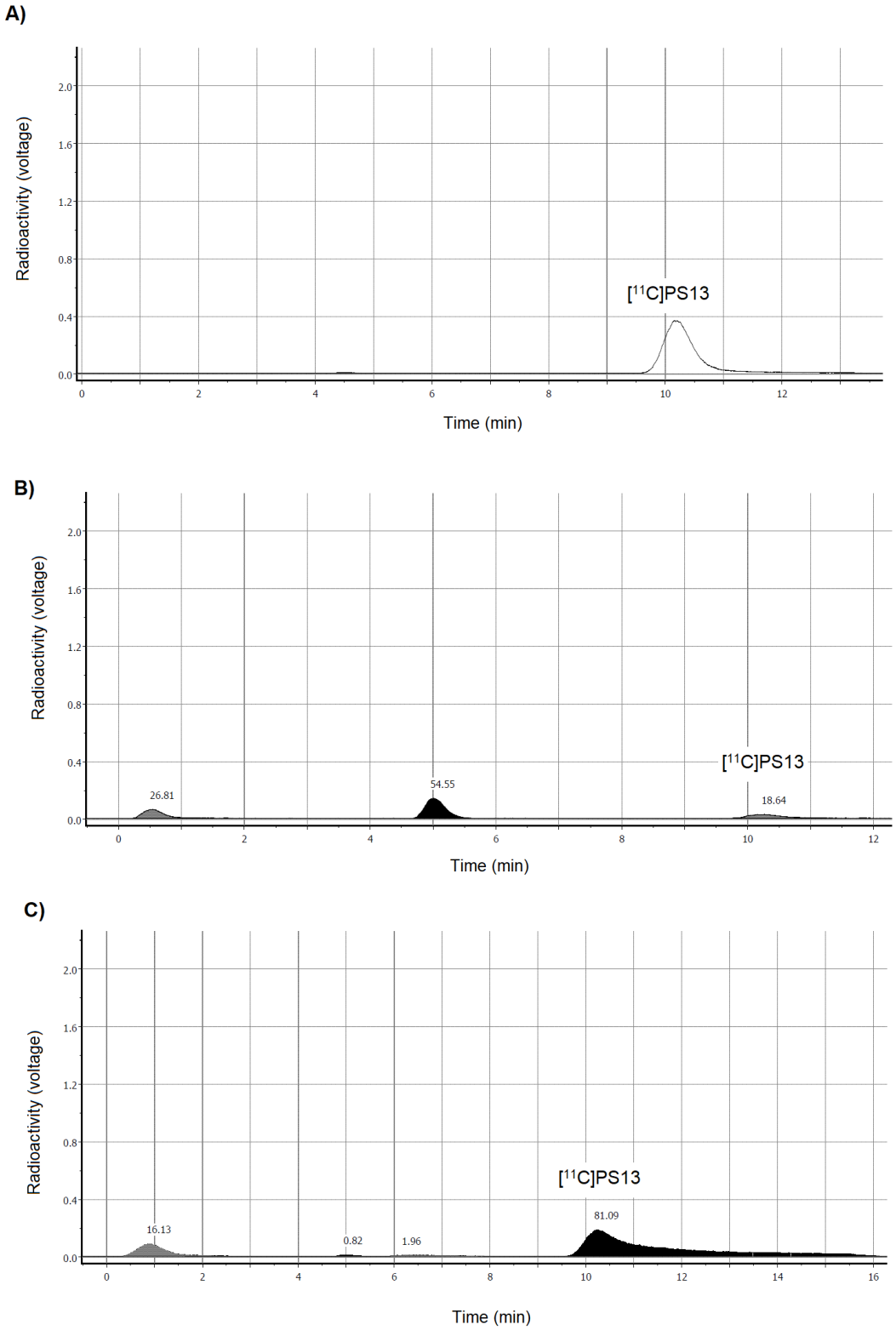

SUPPLEMENTAL FIGURE 4. Radiometabolite analysis in a Mouse 1 (n=2) at 40 min p.i. with [^{11}C]PS13. (A) HPLC chromatogram of [^{11}C]PS13 product following radiosynthesis; HPLC chromatogram with normalized peak analysis from (B) plasma and (C) tumor homogenate.

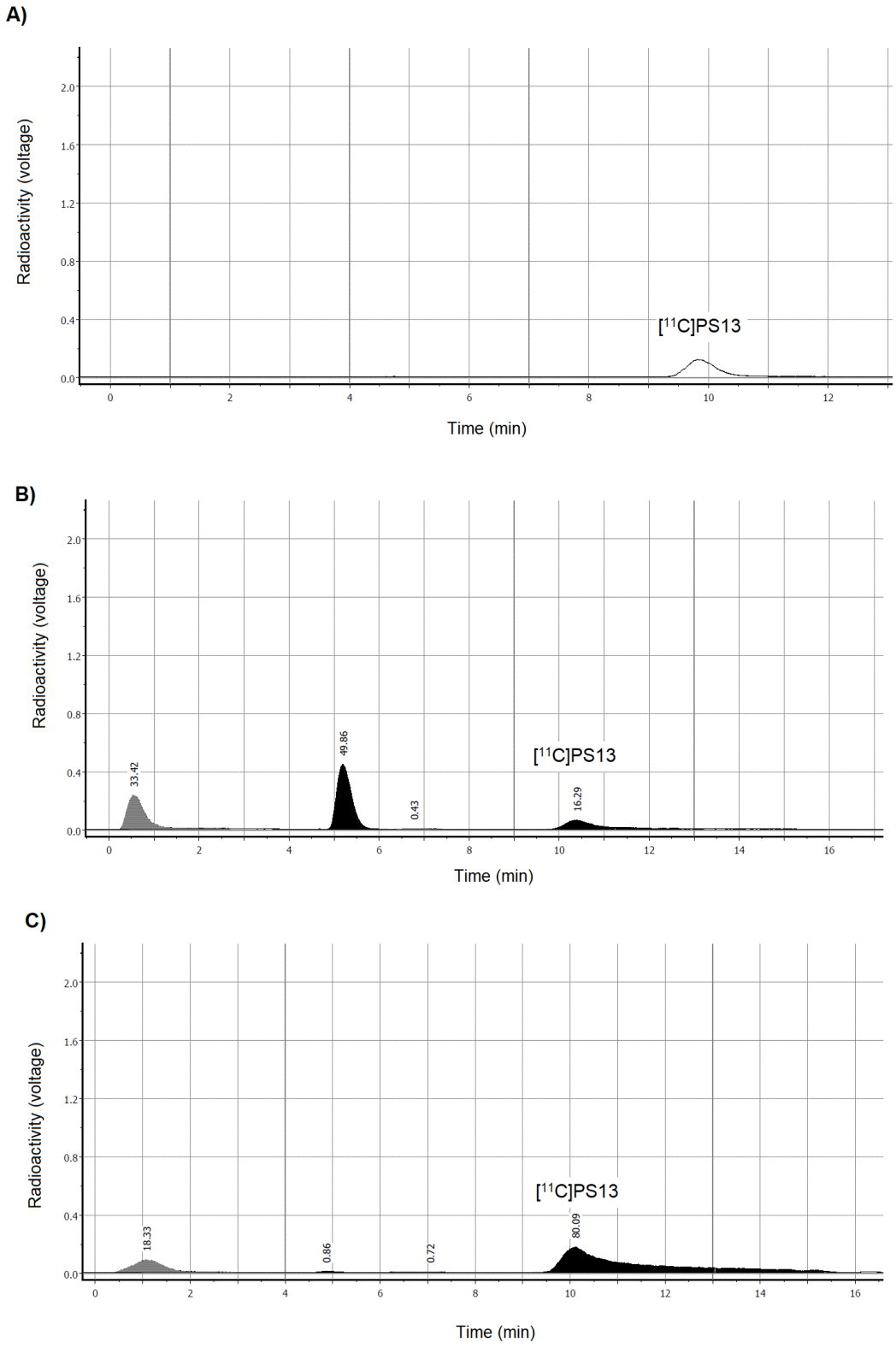

SUPPLEMENTAL FIGURE 5. Radiometabolite analysis in a Mouse 2 (n=2) at 40 min p.i. with [^{11}C]PS13. (A) HPLC chromatogram of [^{11}C]PS13 product following radiosynthesis; HPLC chromatogram with normalized peak analysis from (B) plasma and (C) tumor homogenate.

The Journal of NUCLEAR MEDICINE

Repurposing [^{11}C]PS13 for PET imaging of cyclooxygenase-1 (COX-1) in ovarian cancer xenograft mouse models

Amanda Jean Boyle, Junchao Tong, Sami Zoghbi, Victor W. Pike, Robert Innis and Neil Vasdev

J Nucl Med.
Published online: September 25, 2020.
Doi: 10.2967/jnumed.120.249367

The Journal of Nuclear Medicine is published monthly.
SNMMI | Society of Nuclear Medicine and Molecular Imaging
1850 Samuel Morse Drive, Reston, VA 20190.
(Print ISSN: 0161-5505, Online ISSN: 2159-662X)

SNMMI SOCIETY OF NUCLEAR MEDICINE AND MOLECULAR IMAGING